Journal of Engineering Mathematics **48:** 339–352, 2004.

Numerical evaluation of three-dimensional water impact by the displacement potential formulation

KEN TAKAGI
Department of Naval Architecture and Ocean Engineering, Osaka University, 2-1 Yamadaoka, Suita, Osaka 565-0871, JAPAN (e-mail:takagi@naoe.eng.osaka-u.ac.jp)

Received 7 October 2002; accepted in revised form 18 June 2003

Abstract. The numerical accuracy of the displacement potential approach for a three-dimensional water-impact problem is investigated. An examination of the elliptic paraboloid shows that the boundary-value problem for the displacement potential, as well as the velocity potential, can be solved accurately, even if the panel size of the numerical scheme is no small enough. The numerical accuracy of the position of the contact line is poor. However, the accuracy of the virtual mass is good because of the averaging effect along the contact line. A comparison with Scolan and Korobkin's designed body confirms the accuracy of the drop speed and the penetration displacement. The displacement potential approach is extended to the case of water impact with trapped air. The numerical accuracy of the calculated air pressure in the cavity is confirmed by comparison with an experimental result. With these results, the suitability of the displacement potential approach to the ship-slamming problem is demonstrated.

Key words: displacement potential, inviscid hydrodynamics, ship slamming, water entry

1. Introduction

A typical water-impact problem is the slamming of a ship's bow in high seas. The impact loads experienced need to be properly evaluated for the structural design of the ship. It is obvious that the real impact process of slamming is three-dimensional in nature, and the two-dimensional analysis, the so-called strip method, may not be accurate. In addition, the free-surface shape of a realistic sea has a complex three-dimensional configuration, which makes the three-dimensional effect on slamming even stronger. The three-dimensional impact problem is far from being solved accurately, although numerical methods to solve the hydrodynamic problem have been widely studied over the last two decades.

If we restrict ourselves to the initial stage of water impact and assume that the body is blunt and the deformation of the free surface is gentle, the water-impact problem can be greatly simplified. This means that the body shape close to the initial contact point has a small deadrise angle, which is the main assumption of Wagner's theory [1]. During the initial stage of water impact, the dimensions of the wetted area of the body in the horizontal directions are much greater than the penetration depth. In addition, the free-surface elevation is of the same order as the penetration depth. These restrictions make it possible to linearize the boundary conditions and to impose them on an initially undisturbed free surface.

In the linearized formulation, the deformation of the water surface is identical with the distortion of the bottom of the body. This is a great advantage in solving the water-impact problem in a realistic sea, because we can use a combination of distorted body and flat water-surface instead of flat body and distorted water-surface.

Most studies treat water impact as a two-dimensional problem since the slender-body theory for ship motion requires that the water-impact problem be solved as a part of the inner problem, which is usually two-dimensional. The three-dimensional water-impact theory was studied first by Chuang [2]. He investigated the water impact of cone-shaped bodies. Watanabe [3] studied the pressure distribution on the inclined flat rectangular bottom of a ship penetrating the water surface with a three-dimensional flat-plate formulation. Recently, Toyama [4] presented a theoretical approach to the water-impact problem of three-dimensional bodies. However, Toyama's research objective was limited to a simple-shaped body penetrating a calm water surface.

It is well known that Wagner's problem has a singularity at the intersection between the body surface and the water surface, which makes the numerical solution for a general shape of the body difficult. Takagi [5] employed the displacement potential, which has no singularity at the intersection, to overcome this difficulty. This idea was originally introduced by Korobkin [6]. Howison, Ockendon and Wilson [7] solved the two-dimensional wedge impact with this method and reported good agreement with the exact analytical solution. Takagi [5] extended the method to water impact with trapped air. The displacement-potential approach has a numerical problem, however, when we seek to evaluate the impact force.

This difficulty was successfully resolved by Donguy *et al.* [8]. Takagi and Dobashi [9] also reported resolution of this difficulty in the case of three-dimensional impact with trapped air. On the other hand, Scolan and Korobkin [10] presented the inverse Wagner theory, which gives analytical solutions of the three-dimensional impact problem, although the body shape can only be obtained after solving the problem.

In order to discuss the numerical accuracy of the displacement potential approach to three-dimensional impact on a blunt body of arbitrary shape, numerical solutions of the displacement potential approach are compared with analytical solutions in Section 3. The cases of an elliptic paraboloid at a constant drop speed, and the free fall of designed bodies, which have been reported by Scolan and Korobkin [10] with the inverse Wagner theory, are discussed. In Section 4, besides comparisons with analytical solutions, a numerical solution of the free fall of a circular disk with a circular hollow, in which the air is trapped, is compared with an experiment. Finally, in Section 5 the results obtained are summarized and some directions for further research on the improvement of the displacement potential approach are outlined.

2. Mathematical formulation

The linear theory of water impact was first formulated by Wagner [1]. Since Wagner's solution is an outer solution of the linear theory, it is singular at the contact line between the body and the free surface. Armand and Cointe [11] solve this problem by applying the matched-asymptotic-expansion method. According to their formulation, the preferred perturbation parameter is the ratio between the penetration depth of the body and the horizontal scale of the wetted area of the body. Although the overall problem is composed of an outer problem and an inner problem, only the outer problem is considered here, because the impact force is not affected by the inner solution at the leading order. We use the following non-dimensional space and time coordinates:

$$(x, y, z) = \left(\frac{X}{R}, \frac{Y}{R}, \frac{Z}{R}\right), \quad t = \frac{V_0 T}{H}, \tag{1}$$

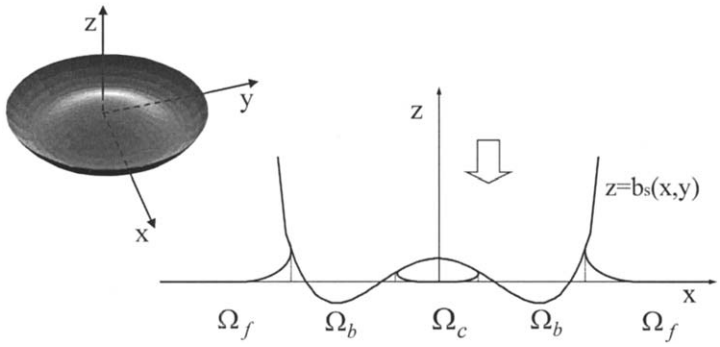

Figure 1. Coordinate system.

where R is the typical horizontal scale of the wetted surface of the body, H is the typical penetration depth and V_0 is the initial drop speed. The xy-plane coincides with the calm water surface, and z is vertically upwards as shown in Figure 1. Linearization is performed by assuming $H/R = \varepsilon << 1$.

We define the non-dimensional drop speed $v(t) = V(t)/V_0$ of the body onto the water surface, which is initially calm. Since the body is assumed to drop freely onto the water, its equation of motion may be

$$m\frac{\mathrm{d}v}{\mathrm{d}t} = m\bar{g} - f \tag{2}$$

with

$$m = \frac{M}{\rho_w R^3}, \quad \bar{g} = \frac{gH}{V_0^2}, \quad f = \frac{FH}{\rho_w V_0^2 R^3}, \tag{3}$$

where M is the mass of the body, ρ_w is the density of water, g is the gravitational acceleration and F is the impact force due to water and trapped-air pressure. The bottom surface of the body is represented by

$$z = \varepsilon b_s(x, y). \tag{4}$$

The impact force acting on the body is obtained by solving an initial-boundary-value problem, known as the Wagner theory. This problem has a singularity at the contact line between the body surface and the water surface. Therefore, we employ the displacement potential, which has no singularity at the contact line. This idea was originally introduced by Korobkin [6]. The displacement potential φ is defined as:

$$\varphi(x, y, z, t) = \int_0^t \phi(x, y, z, \tau)\mathrm{d}\tau, \tag{5}$$

where ϕ is the velocity potential. The displacement potential satisfies Laplace's equation

$$\nabla^2\varphi = 0 \quad \text{for} \quad z < 0. \tag{6}$$

Integrating the linear kinematic boundary condition on the body surface and the free surface for the velocity potential with respect to time, we obtain

$$\frac{\partial\varphi}{\partial z} - \xi(t) - b_s(x, y) = 0 \quad \text{on} \quad z = 0, \quad (x, y) \in \Omega_b, \tag{7}$$

where Ω_b denotes the projection of the wetted part of the body on the plane $z = 0$. Similarly, the dynamic condition for the displacement potential on the free surface is:

$$\varphi = -q(t) \quad \text{on} \quad z = 0, \quad (x, y) \in \Omega_c \cup \Omega_f, \tag{8}$$

where Ω_c denotes the projection of the cavity on the plane $z = 0$ and Ω_f denotes the projection of the outside free surface on the plane $z = 0$. The functions $q(t)$ and $\xi(t)$ are defined as follows:

$$\frac{\mathrm{d}^2 q}{\mathrm{d}t^2} = p(t) \quad \text{for} \ \ (x, y) \in \Omega_c, \tag{9}$$

$$q(t) = 0 \qquad \text{for} \ \ (x, y) \in \Omega_f, \tag{10}$$

$$\frac{\mathrm{d}\xi}{\mathrm{d}t} = -v(t), \quad \xi(0) = 0. \tag{11}$$

Combining (7) and (8), we obtain the following linear boundary condition valid for the overall boundary:

$$(\varphi + q(t)) \left(\frac{\partial \varphi}{\partial z} - \xi(t) - b_s(x, y) \right) = 0 \ \ \text{on} \ z = 0, \ \ (x, y) \in \Omega_c \cup \Omega_b \cup \Omega_f. \tag{12}$$

In order to obtain the physically correct solution, one of the following additional conditions must be satisfied:

$$\varphi \leq -q(t), \ \ \frac{\partial \varphi}{\partial z} - \xi(t) - b_s(x, y) \leq 0 \ \ \text{on} \ z = 0, \ \ (x, y) \in \Omega_c \cup \Omega_b, \tag{13}$$

$$\varphi \leq 0, \ \ \frac{\partial \varphi}{\partial z} - \xi(t) - b_s(x, y) \leq 0 \ \ \text{on} \ z = 0, \ \ (x, y) \in \Omega_b \cup \Omega_f. \tag{14}$$

The condition (13) is switched to (14) at a certain line in Ω_b. A further assumption is that the air in the cavity is adiabatic and that its pressure only depends on time

$$p(t) = \beta \left(\frac{1}{v(t)^n} - 1 \right), \tag{15}$$

$$\beta = \frac{1}{n} \frac{\rho_a}{\rho_w} \left(\frac{c_0}{V_0} \right)^2 \frac{H}{R}, \tag{16}$$

where n is a constant that is dependent on the gas properties; in the case of air, $n = 1{\cdot}4$. The function $v(t)$ is the non-dimensional cavity volume, which is expressed as a fraction of the initial cavity volume, ρ_a is density of the air and c_0 is the speed of sound in air.

The initial-boundary-value problem for the displacement potential is solved by the boundary-element method in space and the Runge-Kutta method in time. It is apparent from the definition that the fluid pressure is obtained by differentiating the displacement potential twice with respect to time. However, differentiation reduces numerical precision. Thus, a new scheme for estimation of the impact force is considered, in which no differentiation is required, although one differentiation is required to determine the pressure distribution.

Once we have solved the initial-boundary-value problem for the displacement potential, the contact line between the body surface and the free surface is known. Thus, we can define a boundary-value problem for the velocity potential

$$\nabla^2\phi_0 = 0 \qquad \text{for } z < 0, \tag{17}$$

$$\phi_0 = -\frac{1}{v(t)}\frac{\mathrm{d}q}{\mathrm{d}t} \qquad \text{for } (x, y) \in \Omega_c, \tag{18}$$

$$\frac{\partial\phi_0}{\partial z} = -1 \qquad \text{for } (x, y) \in \Omega_b, \tag{19}$$

$$\phi_0 = 0 \qquad \text{for } (x, y) \in \Omega_f, \tag{20}$$

where the velocity potential is normalized as $\phi_0 = \phi/v(t)$. The impact force f is obtained by integrating the linear pressure distribution on the wetted body surface and the air pressure in the cavity

$$f = -\int_{\Omega_b}\frac{\partial\phi}{\partial t}\mathrm{d}s + \int_{\Omega_c}\beta\left(\frac{1}{\nu(t)^n} - 1\right)\mathrm{d}s. \tag{21}$$

After some manipulation, the right side of (21) is transformed into

$$f = -\frac{\mathrm{d}}{\mathrm{d}t}\left(\int_{\Omega_b}\phi\ \mathrm{d}s\right) + \frac{\mathrm{d}}{\mathrm{d}t}\left(\frac{\mathrm{d}q}{\mathrm{d}t}\int_{\Omega_c}\mathrm{d}s\right). \tag{22}$$

Substituting (22) in (2) and integrating with respect to time yields

$$v(t) = \frac{m(1 + \bar{g}t) - \frac{\mathrm{d}q}{\mathrm{d}t}\int_{\Omega_c}\mathrm{d}s}{m - \int_{\Omega_b}\phi_0\mathrm{d}s}. \tag{23}$$

The boundary-value problem for the normalized velocity potential ϕ_0 is solved by the boundary-element method. The instantaneous virtual mass $m_a(t)$ is then defined as

$$m_a(t) = -\int_{\Omega_b}\phi_0\mathrm{d}S. \tag{24}$$

3. Numerical scheme

The solution of the boundary-value problem defined by (6), (12), (13) and (14) is represented as a doublet distribution on the plane $z = 0$

$$\varphi(x, y, z) = -\frac{1}{2\pi}\int_{\Omega_c+\Omega_b+\Omega_f}\varphi(x', y', 0)\frac{z}{\{(x - x')^2 + (y - y')^2 + z^2\}^{3/2}}\mathrm{d}S. \tag{25}$$

Ω_f is included in the integral surface for convenience with the numerical scheme. However, the integration in Ω_f makes no contribution. The computational domain $(\Omega_c + \Omega_b + \Omega_f)$ is divided into small elements, and the strength of the doublet is piecewise constant. The computational domain for comparison with the analytical solution in Section 4 is a rectangle. Since the problem in Section 4 is symmetric, only a quarter plane is divided into N rectangular panels of size (Δ_X, Δ_Y). The collocation point is chosen at the centre of panels on which the boundary condition is applied. An example of panelling is depicted in Figure 2.

In Section 5, since the problem is axisymmetric, the computational domain for comparison with experiment is a circle and it is divided radially into N_R pieces. The same panelling and

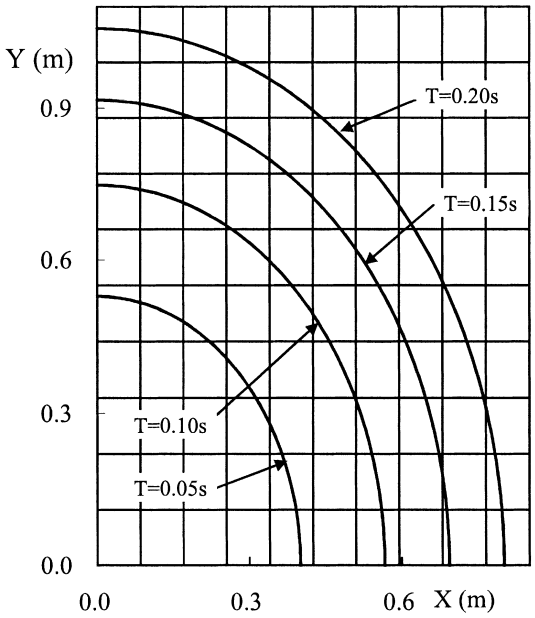

Figure 2. An example of panelling. This panelling is used for the entry of an elliptic paraboloid at a constant velocity, and it corresponds to the large panel ($N = 100$) appearing in Figures 3, 4 and 5. Thick lines are analytical contact lines.

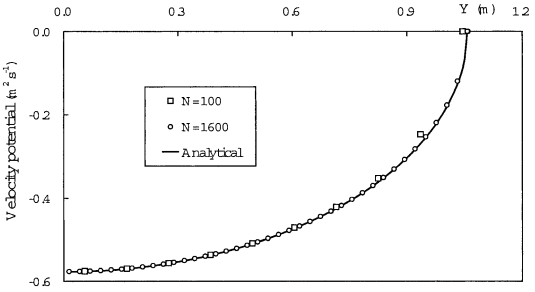

Figure 3. Comparison between the numerical result and the analytical result of the velocity potential along the line $X = 0$ m at the time $T = 0{\cdot}2$ s for $V_0 = 1$ m s^{-1} $A_0 = 0{\cdot}5$ m^{-1}, $B_0 = 0{\cdot}25$ m^{-1}. $N = 100$ is the large panel ($\Delta X = 0{\cdot}085$ m, $\Delta Y = 0{\cdot}11$ m) and $N = 1600$ is the small panel ($\Delta X = 0{\cdot}02125$ m, $\Delta Y = 0{\cdot}0275$ m).

the doublet distribution is also used for the boundary-value problem of the velocity potential defined by (17)–(20). However, in the case of the axisymmetric problem in Section 5, a different panelling with only the wetted surface of the body Ω_b divided into 100 panels at each time steps is used, since the axisymmetric problem is not time-consuming in spite of its intricate algorithm.

Combining the discrete integral equation and the boundary condition (12), we obtain a system of linear equations for the strength of the doublet on each panel. The strength of each doublet is evaluated by the SOR method with the restriction of (13) or (14). In most cases, the residual becomes less than $O(10^{-5})$ after 50 iterations. This scheme is very robust and, even if the Wagner scheme breaks down, the scheme gives a finite value.

The contact line between the body surface and the free surface is automatically decided with this scheme, when the strength of the doublet is evaluated. The contact line is a link of edges of panels on which the magnitude of the velocity potential is $-q(t)$, *i.e.*, the velocity potential inside this line is less than $-q(t)$. However, the numerical accuracy of the position of the contact line is not sufficient, since the accuracy of the position of the contact line is of the same order as the size of the panels.

There are many ways to improve the accuracy for defining the contact line. For example, fine panels can be fitted along the contact line. However, this process makes the numerical scheme complicated and possibly less robust. The present scheme is very simple and very

useful for engineering applications. The accuracy of the definition of the contact line will be discussed again in the following sections.

4. Comparison with analytical solutions

Scolan and Korobkin [10] developed some analytical solutions of the three-dimensional impact problem by solving the inverse Wagner problem. In order to investigate the accuracy of the solutions by the displacement-potential approach, comparisons with their solutions are made.

4.1. Entry of an elliptic paraboloid at constant velocity

The problem of an elliptic paraboloid entering initially calm water at a constant velocity is considered. The position of the moving body at time t is given by the equation

$$Z = A_0 X^2 + B_0 Y^2 - V_0 T, \tag{26}$$

where A_0 and B_0 are given constants.

A comparison between the numerical result and the analytical result of the velocity potential is shown in Figure 3. The numerical result for the small panel is in excellent agreement with the analytical result. Even in the case of a large panel, although some discrepancy is seen near the contact line, agreement with the analytical result is very good.

A comparison of the contact lines in Figure 4 shows that agreement between the large panel and the analytical solution is poor. In the worst case ($T = 0{\cdot}05$ s, $N = 100$), the discrepancy is 17·4% of the width of the wetted surface, with the numerical contact line being a staircase pattern with its smallest step corresponding to the size of the panel. The contact line depicted in Figure 4 is a link of edges of panels on which the magnitude of the velocity potential is zero.

The accuracy of numerical results for the virtual mass is fairly good, even if the panel size is large, as shown in Figure 5. In the worst case ($T = 0{\cdot}05$ s, $N = 100$), the discrepancy is 4·1% of the exact value.

Since the magnitude of the velocity potential near the contact line approaches zero, inaccurate definition of the contact line does not seriously affect the result of the integral (24). In addition, since the numerical contact line crosses the analytical contact line many times, the averaging effect of integration causes the results to converge. In fact, the difference between the area of the numerical wetted surface and that of the exact wetted surface is 9·3% in the worst case, and the magnitude of the velocity potential at edge panels is about one-half of the average magnitude in the wetted surface. These two results explain the discrepancy of the virtual mass, which is 4·1% in the worst case.

This result suggests that the numerical accuracy of the drop speed may be good when we calculate the free fall motion, since drop speed is directly calculated from the virtual mass. Moreover, it is expected that the numerical accuracy of the penetration depth is better than the accuracy of the drop speed because of the averaging effect, which erases the fluctuations of the position of the numerical contact line in time. These predictions will be demonstrated in the next section by comparisons with analytical results for designed bodies.

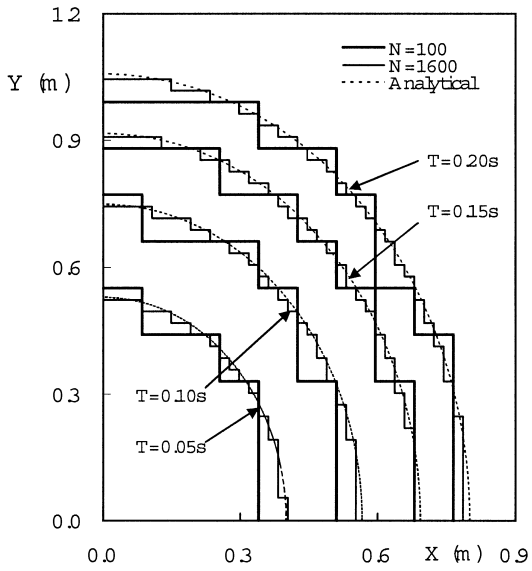

Figure 4. Contact lines at different time instants.

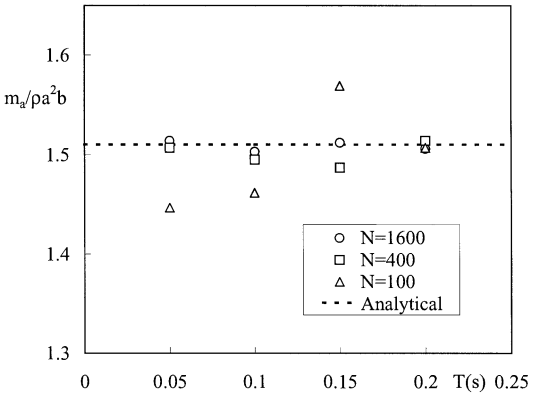

Figure 5. Non-dimensional virtual mass $m_a/\rho a^2 b$ by the displacement potential approach at different time instants. $N = 400$ is the medium panel ($\Delta X = 0{\cdot}0425$ m, $\Delta Y = 0{\cdot}055$ m). The analytical value obtained by Scolan and Korobkin [10] is 1·510.

4.2. FREE FALL OF DESIGNED BODIES

Strictly speaking, the designed-body case is not an analytical solution, since the solution is evaluated by performing an integral. However, since this integral has no singularity and is not difficult to evaluate accurately, it may be called an analytical solution when we compare it with the numerical solutions.

The designed bodies used here have an elliptic contact line whose position at an instant t is described by the equation

$$\frac{X^2}{A^2(t)} + \frac{Y^2}{B^2(t)} = 1. \tag{27}$$

It is convenient to introduce the elliptic eccentricity $e(t) = \sqrt{1 - (A(t)/B(t))^2}$. In the axisymmetric case $e(t) \equiv 0$.

In the following discussion, we use designed bodies of $e(t) \equiv 0{\cdot}9$ and $e(t) \equiv 0{\cdot}1$. The shapes of the designed body are found in Figure 11 of [10]. Calculations were performed with $V_0 = 4{\cdot}43$ m s^{-1}, $M = 100$ Kg and $g = 9{\cdot}81$ m s^{-1}. The drop speed of the designed body of $e = 0{\cdot}9$ is shown in Figure 6. Agreement between the small-panel result and the analytical result is very good, and the result for the large panel is in fairly good agreement with the analytical result. The same tendency can be seen in Figure 7 for $e = 0{\cdot}1$.

Figures 8 and 9 show the variation of penetration depth with respect to time. Agreement between the numerical and analytical results is excellent, even for the case of a large panel. The good agreement is considered to be due to the averaging effect as explained previously.

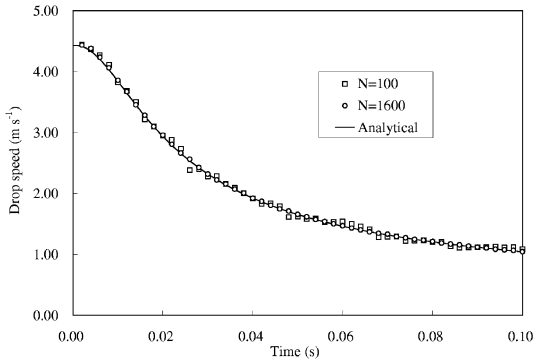

Figure 6. Drop speed of the designed body $e = 0{\cdot}9$. $N = 100$ is the large panel ($\Delta X = 0{\cdot}12$ m, $\Delta Y = 0{\cdot}07$ m) and $N = 1600$ is the small panel ($\Delta X = 0{\cdot}03$ m, $\Delta Y = 0{\cdot}0175$ m).

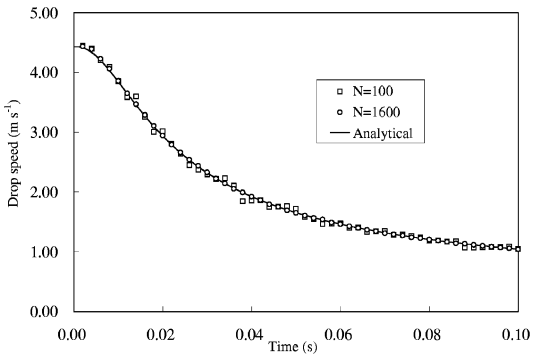

Figure 7. Drop speed of the designed body $e = 0{\cdot}1$. $N = 100$ is the large panel ($\Delta X = \Delta Y = 0{\cdot}08$ m) and $N = 1600$ is the small panel ($\Delta X = \Delta Y = 0{\cdot}02$ m).

Finally, we show the time variation of the semi-axis $A(t)$ and $B(t)$ in Figures 10 and 11, respectively. Agreement between the small-panel result and the analytical result is fairly good, but that between the large panel result and the analytical result is very poor. The reason is that semi-axes $A(t)$ and $B(t)$ of the numerical result are obtained from the positions of the contact line at $Y = 0$ and $X = 0$, respectively, and do not include any averaging effect.

These results confirm that the displacement-potential approach is accurate if we use the small panel. If we only need the penetration depth, even the large panel gives an accurate result. However, if we need an accurate position of the contact line, for example when we calculate the impact force or the impact pressure, even the small panel gives an inaccurate result.

5. Comparison with experimental results

A free-fall test of an axisymmetric body with attached cavity was carried out by Dobashi and Takagi [12]. They show only the time history of the pressure in the cavity. Sequential photographs of the intersection lines are shown in this paper.

5.1. Condition of experiment

The body has a circular hollow at the bottom. We assume that this hollow guarantees cavity formation in advance. The bottom shape of it is represented by a quadratic function $Z = H[(X^2 + Y^2)/L^2 - 1]^2$, where $H = 0{\cdot}01$ m and $L = 0{\cdot}07$ m. The mass of the body is 3·38 Kg.

We prefer the axisymmetric body, because if we use two-dimensional body, it is difficult to prevent ventilation of the cavity from the gap between the tank wall and the body surface. In addition, it is easy to construct the experimental body shape accurately, and the numerical calculation is very accurate if the body is axisymmetric.

The measured drop speed of the model is 0·92 m s^{-1} at the moment of impact with the undisturbed water surface. The motion of the body is restrained in the vertical direction by

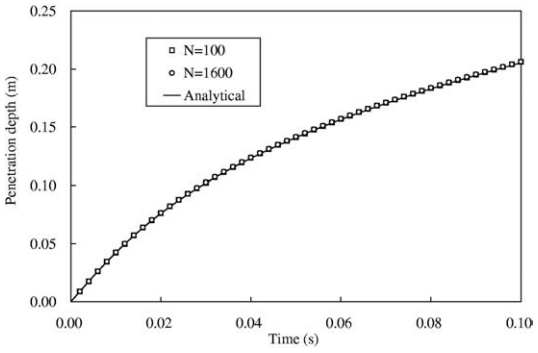

Figure 8. Time variation of the penetration depth for $e = 0{\cdot}9$.

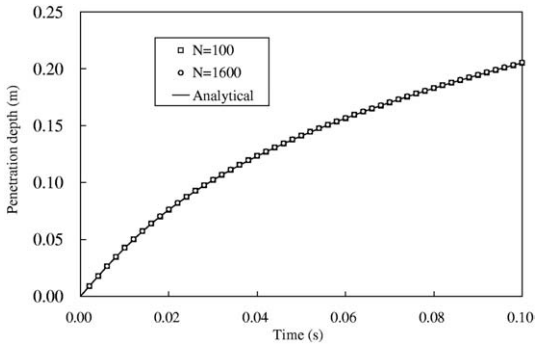

Figure 9. Time variation of the penetration depth for $e = 0{\cdot}1$.

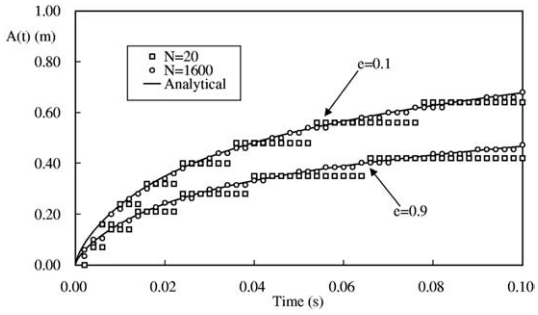

Figure 10. Time variation of semi-axis $A(t)$ for $e = 0{\cdot}9$ and $e = 0{\cdot}1$.

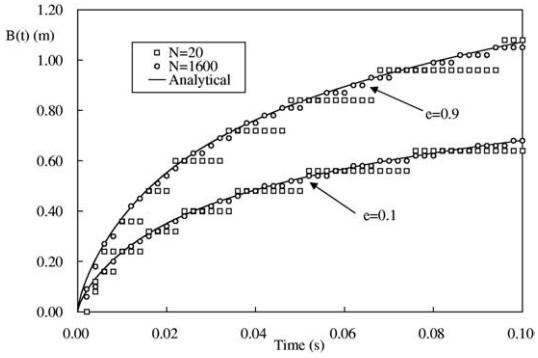

Figure 11. Time variation of semi-axis $B(t)$ for $e = 0{\cdot}9$ and $e = 0{\cdot}1$.

guide rails, and the body falls onto the calm water surface in a water tank ($0{\cdot}45 \times 0{\cdot}45 \times 0{\cdot}45$ m).

Only the air pressure in the cavity is measured, because it is difficult to measure the pressure on the wetted surface of the body. The difficulty arises because the pressure change near the spray root is very rapid – *i.e.*, the pressure varies from maximum to zero in a very small space, which is of the order of the thickness of the spray. Thus, a pressure sensor whose diameter is much larger than the spray thickness may not register a variation of pressure in such a small space. Another problem is that usually the lowest resonance frequency of the pressure sensor for the low-pressure measurement (the maximum pressure for this experiment may be less than 100 KPa.) is not high enough for the impact pressure, since it is proportional to the capacity of the pressure sensor.

The air pressure in the cavity is measured with a pressure gauge mounted at the centre of the hollow. The error range of the experiment is indicated in Figure 12 by an error bar, which is based on an uncertainty analysis of the measurement system. A mirror is set under the water tank to observe the formation of the cavity and the spray, and sequential photographs are taken with the mirror. The time interval of the sequential photos is not constant, since the camera shutter is controlled by photo sensors, which are placed at intervals of 0·001 m. The first photo

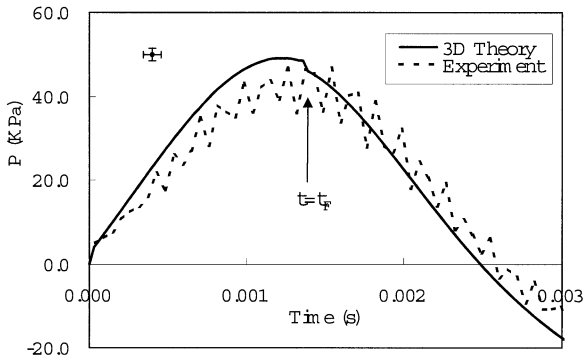

Figure 12. Comparison between the numerical result and the experimental result of the air pressure in the cavity.

sensor is adjusted so that the first photo is taken at the instant when the bottom of the body just touches the undisturbed water surface.

5.2. Results of experiment

Figure 12 compares the numerical result with the experimental result for the air pressure in the cavity. There is a small fluctuation on the time history of the experimental data. This fluctuation is thought to be due to vibration of the pressure gauge, since the natural period of the pressure gauge is almost the same as the period of the fluctuation. Except for this fluctuation, agreement between the numerical and experimental results is good up to the time $t = t_F$. The discrepancy between the averaged experimental value – *i.e.*, after removing the small fluctuation – and the numerical estimation at the pressure peak is 13% of the peak value. At the time $t = t_F$, the Wagner scheme fails as stated in the Appendix. However, the numerical calculation still gives reasonable results after this time.

Figure 13 shows sequential photos of the bottom surface of the drop body during the initial stage of the impact. The photos are taken from below. While they may not be sufficient to confirm the free-surface elevation of the numerical result, since they are taken from only one direction, the following observation can be made.

The contact lines are visible on the body surface, even though their exact positions are not clear enough because of the spray. It seems that the contact lines are axisymmetric, while the spray is not, and a circular cavity is formed at the beginning of the impact. Ventilation does not occur, even though the pressure in the cavity is negative, as seen in the last shot of Figure 13. These photos imply that the assumptions used in the present theory are reasonable. However, in order to confirm the numerical result of the wave elevation, we may need data in the vertical plane.

6. Conclusion

The numerical accuracy of the displacement approach for the three-dimensional water impact problem has been investigated. The numerical scheme is applicable for a blunt body of arbitrary shape falling onto the water surface. An examination of the elliptic paraboloid shows that boundary-value problems for displacement potential and velocity potential can be solved accurately, even if the panel size of the numerical scheme is large. On the other hand, the numerical accuracy of the position of the contact line is poor, since the lower limit of the error

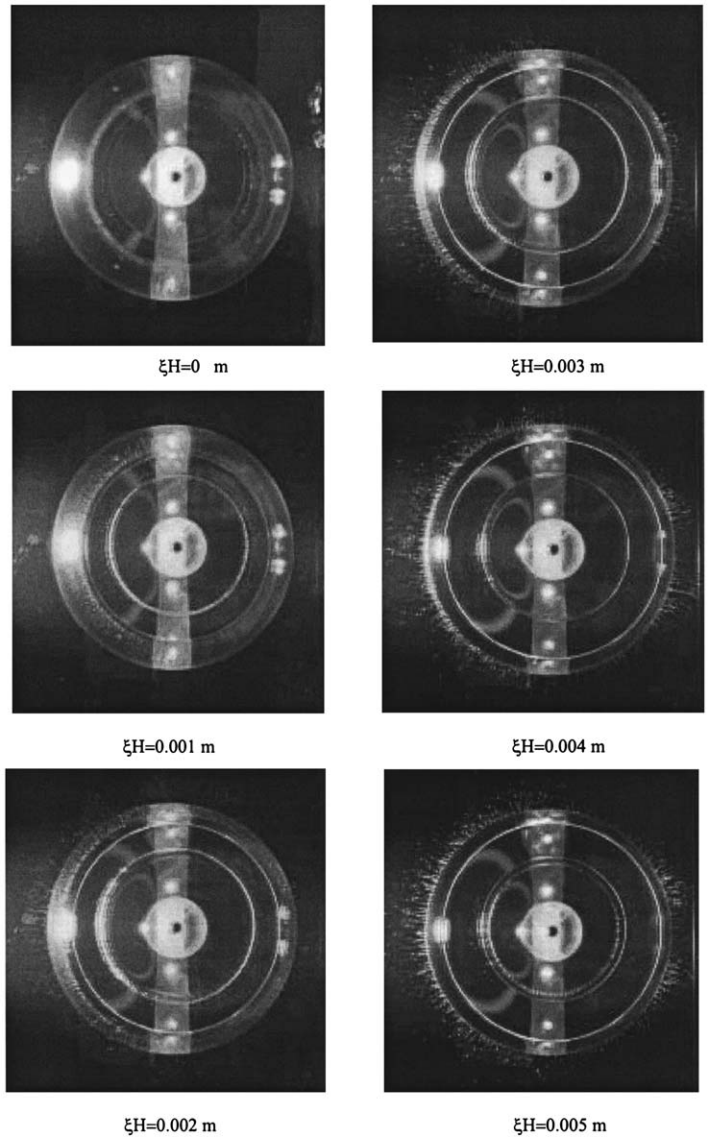

Figure 13. Sequential photos of the contact lines.

of the position cannot be less than the panel size. Accuracy of the virtual mass is good because of the averaging effect and the characteristic of the pressure distribution along the contact line. This result implies that we can perform an accurate evaluation of the drop speed of the body. Comparison with Scolan and Korobkin's designed body confirms the accuracy of the drop speed and shows that we can obtain a much better estimation of the penetration displacement than that of the drop speed.

Estimation of a ship's strength against water impact is important from an engineering point of view. When we discuss ship structural response, a mass-and-spring system with two degrees of freedom is often used – see for example [9]. In this model, the global responses, such as heave, pitch and distortion modes are represented as a large mass and a hard spring, and the response of the local structure is represented by a small mass and a weak spring. The equation

of motion of this model requires the impulse due to water impact as an exciting force, and induced stress is estimated from the displacement of the body. These values are accurately estimated by the displacement potential approach.

For more realistic modelling of the ship structure and estimation of the structural response, modal analysis will be used. In this case, the advantage of the displacement approach may still be valid. However, if we need fluid-dynamic characteristics, such as the pressure distribution, the peak pressure and the spray thickness, the numerical results may be unreliable because of inaccurate differential operations due mainly to the inaccuracy of the position of the contact line.

The displacement-potential approach has been extended to the case of water impact with trapped air. The numerical accuracy of the air pressure in the cavity is confirmed by comparison with an experimental result. Sequential photos of the experiment supports the assumptions of the linear formulation of the blunt body impact with an attached cavity. These results suggest the applicability of the displacement-potential approach to the more realistic problem of a ship slamming with trapped air in rough sea.

Although the displacement-potential approach is appropriate for evaluation of the water-impact problem, further work may be necessary to improve calculation of the exact position of the contact line for an accurate estimation of the pressure distribution. The linear formulation works very well during the early stage of impact. However, it is necessary to study how to connect this theory to the conventional ship-motion theory in the time domain, to clarify the effects of the gravity and the non-linearity of the body-boundary condition. The failure of Wagner's scheme is another difficulty, which may require further modelling of fluid motion along the contact line.

Acknowledgement

The author is grateful to Dr. Y.M. Scolan and Dr. A.A. Korobkin for providing digital data of their numerical results in [10].

Appendix: Problem of the Wagner scheme

A problem occurs at the time $t = t_F$ for the three-dimensional theory in Figure 12 when the free surface in the cavity cannot be attached at the intersection, and the Wagner scheme fails. The same situation has been reported by Korobkin [13] in the case of two-dimensional theory. According to his two-dimensional theory, we investigate the details of this phenomenon.

If the drop speed of the body is a constant V_0, the non-dimensional elevation η of the outer free surface is

$$\eta(x,t) = \left[\frac{2}{\pi}\int_{x_a(t)}^{x_c(t)} y_b(x',t)\frac{x'\sqrt{(x_c(t)^2-x'^2)(x'^2-x_a(t)^2)}}{x'^2-x^2}\mathrm{d}x' - D_c(t)\right] \times\left[(x^2-x_c(t)^2)(x^2-x_a(t)^2)\right]^{-1/2} \tag{A1}$$

and of the inner free surface is

$$\eta(x,t) = \left[-\frac{2}{\pi}\int_{x_a(t)}^{x_c(t)} y_b(x',t)\frac{x'\sqrt{(x_c(t)^2-x'^2)(x'^2-x_a(t)^2)}}{x'^2-x^2}\mathrm{d}x' + D_c(t)\right] \times\left[(x^2-x_c(t)^2)(x^2-x_a(t)^2)\right]^{-1/2}, \tag{A2}$$

where $x_c(t)$ denotes the intersection point between the outer free surface and the body surface, $x_a(t)$ denotes the intersection point between the inner free surface and the body surface, and function $y_b(x,t) = (x^2-1)^2 - t$ denotes the instantaneous body shape. $D_c(t)$ is evaluated from the asymptotic form of vertical velocity far from the body. The vertical displacements of both the outer free surface and the inner one are bounded if

$$D_c + A_c^2(B_c - 1) + A_c(B_c - 1)^2 + \frac{A_c^3}{2} - A_c t = 0, \tag{A3}$$

$$D_c + A_c^2(B_c - 1) - A_c(B_c - 1)^2 - \frac{A_c^3}{2} + A_c t = 0, \tag{A4}$$

where $A_c = (x_c^2 - x_a^2)/2$ and $B_c = (x_c^2 + x_a^2)/2$. These two equations lead cubic equation of A_c^2

$$A_c^6 - 2tA_c^4 + 2D_c^2 = 0 \tag{A5}$$

It is found that if $D_c > 4(t/3)^{3/2}$, A_c^2 has no positive root. This corresponds to the time $t = t_F$. After this instant, (A3) and (A4) cannot be satisfied simultaneously. Thus, we must weaken the unbounded condition at the intersection point in the cavity $x = x_a(t)$. This problem and how to continue the simulation after the time instant t_F are discussed in detail by Takagi and Dobashi [9].

References

1. H. Wagner, Über Stoss und Gleitvergänge an der Oberfläche von Flüssigkeiten. *Zeitschr. Angew. Math. Mech.* 12 (1932) 193–215.
2. S.L. Chuang, Theoretical investigations on slamming of cone-shaped bodies. *J. Ship Res.* 13 (1969) 276–283.
3. I. Watanabe, Effects of the three-dimensionality of ship hull on the wave impact pressure. *J. Soc. Naval Arch. Japan* 162 (1987) 163–174.
4. Y. Toyama, Flat plate approximation in the three-dimensional slamming. *J. Soc. Naval Arch. Japan* 179 (1996) 271–279.
5. K. Takagi, Three-dimensional slamming of a distorted plate. In: J.S. Chung, B.M. Das, T. Matsui and H. Thiel (eds.), *Proc. of Int. Symposium of ISOPE, Honolulu*, Vol. 1 (1997) pp. 237–244.
6. A.A. Korobkin, Formulation of penetration problem as a variational inequality. *Din Sploshnoi Sredy* 58 (1982) 73–79.
7. S.D. Howison, J.R. Ockendon and S.K. Wilson, Incompressible water-entry problem at small deadrise angles. *J. Fluid Mech.* 222 (1991) 215–230.
8. B. Donguy, B. Peseux and E. Fontaine, On the ship structural response due to slamming loads. In: E. Onate, G. Bugeda and B. Suarez (eds.), *European Congress on Computational Methods in Applied Sciences and Engineering, ECCOMAS 2000, Barcelona, 11-14 September 2000*, CIMNE Barcelona Publication (2000) pp. 1–15.
9. K. Takagi and J. Dobashi, Influence of trapped air on the slamming of a ship. *J. Ship Res.* (2003) (To appear).
10. Y.M. Scolan and A.A. Korobkin, Three-dimensional theory of water impact. Part 1. Inverse Wagner problem. *J. Fluid Mech.* 440 (2001) 293–326.
11. J.L. Armand and R. Cointe, Hydrodynamic impact analysis of a cylinder. In: J.S. Chung, S.K. Chakrabarti, H. Maeda and R.E. Jeffreys (eds.), *Proc. of 5th Int. OMAE Symposium, Tokyo* Vol. 1 (1986) pp. 250–256.
12. J. Dobashi and K. Takagi, Water entry problem of an axisymmetrical body with attached cavity. In: S. Naito and H.S. Choi (eds.), *Proc. of 4th Japan-Korea Joint Workshop on Ship and Marine Hydrodynamics, Fukuoka* (1999) pp. 15–22.
13. A.A. Korobkin, Entry Problem for body with attached cavity. In: V. Bertram (ed.), *Proc. of 11th Int. Workshop on Water Waves and Floating Bodies, Hamburg* (1996) pp. 93–96.